Please cite this article as: Finnegan W., Goggins J., 'Numerical simulation of linear water waves and wave-structure interaction'. *Ocean Engineering* 43 (2012) 23–31

Numerical Simulation of Linear Water Waves and Wave-Structure Interaction

William Finnegan[a], Jamie Goggins[a,b,*]

[a] *College of Engineering and Informatics, National University of Ireland, Galway, Ireland*
[b] *Ryan Institute for Environmental, Marine and Energy Research, National University of Ireland, Galway, Ireland*
** Tel: +35391492609, Fax: +35391494507, E-mail: jamie.goggins@nuigalway.ie*

Abstract: One of the main stages in the design of wave energy converters (WEC's) is the numerical modelling of a given converter. In this paper, the numerical simulation of both linear deep water waves and linear waves for the finite depth case are explored using computational fluid dynamics (CFD), to aid in this design stage. The CFD software package described in this paper is the commercial finite volume package ANSYS CFX (Release 12.1). The results of parametric studies, which were performed in order to optimise the CFD model, are detailed and a guide to creating a model that produces the desired waves is presented. The model was validated in two ways: (a) the wave created was compared to wavemaker theory (WMT) and (b) the water particle velocity and elevation of the wave was compared to linear, Airy, wave theory (LWT) for deep water waves. It was also found that wave generation in ANSYS CFX using a flap-type wavemaker was restricted to a low normalised wavenumber, k_0h. In order to increase this restriction, the hinge of the wavemaker was raised and, with this alteration, it is possible to generate deep water linear waves. A case study of a real world application of wave-structure interaction, employing this methodology, is also explored.

Keywords: *ANSYS CFX, Computational fluid dynamics, Deep water waves, Linear (Airy) wave theory, Wave energy, Wavemaker theory.*

Nomenclature:

A	Wave amplitude	*m*	M	Mass of the structure	*kg*
a	Radius of a vertical cylinder	*m*	p	Pressure	*Pa*

a_m	Added mass		p_0	Coefficient	
b	Draft of a vertical cylinder	*m*	q_i	Volume fraction of the fluid i	
d	Water height at the SWL	*m*	T	Wave period	*s*
g	Acceleration due to gravity	m/s^2	t	Time	*s*
F_i	Force i-component	*N*	S	Stroke length	*m*
F_{ext}	Excitation force	*N*	s	Scaling factor	
F_H	Hydrodynamic force	*N*	U(y)	Prescribed horizontal velocity of the wavemaker	*m/s*
F_{hs}	Hydrostatic force	*N*	u_i	Flow velocity i-component	*m/s*
F_R	Radiation force	*N*	v	Water particle velocity	*m/s*
f	Frequency (1/T)	s^{-1}	x	Distance from wavemaker	*m*
H	Wave height	*m*	y	Increases from the SWL with depth	*m*
$H_m^{(1)}$	Hankel function of the first kind of order *m*		ε_0	Initial phase angle	
h	Height of wavemaker flap from hinge to SWL	*m*	ξ	Separation constant	
I_m	Modified Bessel function of the first kind of order *m*		μ	Viscosity	*Pa.s*
J_m	Bessel function of the first kind of order *m*		ρ	Fluid density	Kg/m^3
k_0	Wavenumber	m^{-1}	φ	Velocity potential	ms^{-1}
l	Height of wavemaker flap hinge from base of model	*m*	ω	Wave angular frequency	s^{-1}
L_0	Wavelength	*m*			

1. Introduction

In the design of any floating or fixed marine structure, it is vital to test models in order to understand the fluid/structure interaction involved. Inevitably laboratory experiments will be carried out in a wave tank or wave basin, followed by tests on scale models in real sea conditions. However, with the developments in computational fluid dynamics (CFD) software, it is now possible to carry out

inexpensive and relatively quick initial studies. That is, provided that the numerical model used is representative of the real life environment.

The numerical models used to model wave-tanks are known as numerical wave tanks (NWT's). NWT's are developed using a variety of numerical techniques, including the boundary volume method (BEM), the finite element method (FEM) and the finite difference method. In a NWT, a wave is generated at the input boundary and damped out near the output boundary.

Kim et al (2001) and Park et al (2004) numerically simulated 3-D non-linear multi-directional waves using a finite difference method. The waves were generated using a numerical wavemaker by specifying the water particle velocities at the wavemaker boundary. Koo and Kim (2004) expanded the process to fluid-structure interaction in order to explore the effects of a nonlinear wave on a freely floating body for the 2-D case. Sun and Faltinsen (2006) developed a 2-D numerical tank using the boundary element method in order to simulate the impact of a horizontal cylinder on the free surface. Ning and Teng (2007) used a three-dimensional higher order boundary element model to simulate a fully nonlinear irregular wave tank. Ning et al (2008) expanded this study to infinite water depth for nonlinear regular and focused waves. On the other hand, Yan and Lui (2011) developed a 3-D numerical wave tank using a high-order boundary element method (HOBEM) in order to simulate nonlinear wave-wave and wave-body interactions. The fluid motion inside a sphere was an example of wave-body interaction that they explored.

Wu and Hu (2004) used a FEM numerical tank with a wavemaker to simulate the nonlinear interaction between water waves and a floating cylinder. Hadzic et al (2005) created a 2-D NWT using a commercial CFD software package to explore the motion of a floating rigid body with up to six degrees of freedom as it is subjected to large amplitude waves. Turnbull et al (2003) investigated the effects of inviscid gravity waves on a submerged fixed horizontal cylinder in a 2-D FEM numerical wave tank. Agamloh et al (2008) used a commercial CFD software package to develop a 3-D numerical wave tank, which allowed fluid-structure interaction of a water wave and a cylindrical ocean wave energy device to be explored. Both the response of a single device and the response of an

array of devices were investigated. Sriram et al (2006) used a piston type wavemaker to generate 2-D nonlinear waves using FEM. Sriram et al (2006) used a cubic spline approximation with the finite element approach when discretising the domain and had a fully reflecting wall at the end of the boundary. Contento (2000) used a 2-D numerical wave tank, which was based on the BEM technique, to simulate the nonlinear motions of arbitrary shaped bodies in order to develop improved seakeeping techniques. Mousaviraad et al (2010) developed a harmonic group single run seakeeping procedure, which was solved using a general purpose unsteady Reynolds averaged Navier-Stokes (URANS) solver. A linear potential solution was specified at the input boundary in order to generate linear input waves. Liang et al (2010) also explored the use of a piston type wavemaker to generate an irregular wave train using FEM. In 2008, Lal and Elangovan (2008) explored the CFD simulation of linear water waves for a flap type wavemaker using the same finite volume package described in this paper. However, the dimension of the model was taken as an experimental wave tank and simulations were only carried out for the shallow water case.

In this paper, an efficient NWT model is developed by altering its overall dimensions, as shown in Figure 1. In particular the overall height, the base length and mesh setup are varied to obtain an efficient model. These dimensions are dependent on the period of the desired deep water waves. The model works the same way as an experimental wave tank. The waves are generated at the model input boundary using a flap-type wavemaker and there is a sloped beach in place at the model output boundary in order to damp out the wave, which can be seen in **Fig. 1**. The CFD software package used in this analysis is ANSYS CFX (ANSYS, 2009). It uses a finite volume method in order to solve the Reynolds Averaged Navier-Strokes equations (RANSE), which accounts for turbulence and viscosity. When the analysis is extended to fluid-structure interaction, ANSYS Mechanical is used in conjunction with CFX as a motion solver.

In this paper, 2-dimensional CFD models are validated using wavemaker theory (WMT) for deep water waves. The experimental validation of WMT was achieved by Ursell et al (1960) using an experimental wave tank. Furthermore, the water particle velocities determined by the CFD model are compared to linear, Airy, wave theory (LWT). Therefore, the waves generated by the model will be

validated by comparing to both LWT and WMT. Thus, the main objective of this paper is to present a guide to designing a CFD model that can accurately produce both linear deep water waves and linear finite depth water waves. Furthermore, the model outlined in this paper will represent an optimised wave tank model, as its overall dimensions will be dependent on the period of the desired waves. In order to achieve this model, a number of convergence tests were carried out. Finally, a case study of a real world application of the methodology derived is undertaken. It is an analysis of the interaction between a linear deep water wave and a floating truncated vertical cylinder.

2. Methodology

The CFD model created in this paper is similar in set-up to that of an experimental wave tank. However, the model dimensions are to be recalculated in order to optimise the model dependant on the period of the desired waves. An illustration of the dimensioning is shown in **Fig. 1**, where d is the height of the still water level (SWL), S is the stroke length of the wavemaker and H is the height of the generated wave. Furthermore, since the generated waves are to be compared to LWT, the waves created are assumed to be of small amplitude relative to their length. Small amplitude waves are defined by the steepness relation $H/L_0 \leq 0.03$ (Ursell et al, 1960), where L_0 is the wavelength. The response of wave energy converters (WEC's) to small amplitude waves is of interest as their performance needs to be optimised when the resource is at its least. In other words, the WEC should be tuned to the expected properties of the dominant small amplitude waves.

The set-up for the CFD model is divided into three stages: (1) the geometry setup, which defines the physical dimensions of the model, (2) the mesh setup, where a mesh is created and is refined at the still water level (SWL) to capture the free surface accurately, and (3) the wave water, or physics, setup, which defines the analysis type, the domain setup, the motion of the wavemaker, the initial water height and other characteristics of the water and air-water interaction. In defining the domain set-up, a number of assumptions are included. The surface tension at the air-water interface is assumed to be negligible. The air is specified to a temperature of 25°C and, therefore, its density is

specified to be 1.185 kg/m^3. Furthermore, an isothermal heat transfer model is specified, which is homogeneous. The fluid (water) temperature is defined as 25°C and its density is given as 1030 kg/m^3 to represent salt water.

The top of the model has an opening boundary condition, which allows air to pass through. The boundary condition at the wavemaker is a wall with a specified displacement, which is inputted using the ANSYS CFX expression language (CEL) (ANSYS, 2009). There are symmetry boundary conditions specified for the adjacent sides, in order to create a model that is infinitely wide, and the remaining boundaries are assigned a static wall boundary condition.

2.1. The governing equations

The method on which the solver in ANSYS CFX is based on is the finite volume technique (ANSYS, 2009). This technique divides the region of interest into sub-regions and discretises the governing equations in order to solve them iteratively over each sub-regions. Therefore, an approximation of the value of each variable at points throughout the domain is achieved.

The governing equations that need to be solved by the ANSYS CFX solver is the mass continuity equation (Versteeg and Malalasekera, 1995), which is given as:

$$\frac{\partial \rho}{\partial t} + \frac{\partial \rho u_1}{\partial x} + \frac{\partial \rho u_2}{\partial y} = 0 \qquad (1)$$

and the Navier-Stokes equations (Versteeg and Malalasekera, 1995), which are given as:

$$\rho\left(\frac{\partial u_1}{\partial t} + u\frac{\partial u_1}{\partial x} + v\frac{\partial u_1}{\partial y}\right) = -\frac{\partial p}{\partial x} + 2\mu\frac{\partial^2 u_1}{\partial x^2} + \frac{\partial}{\partial y}\left(\mu\left(\frac{\partial u_1}{\partial y} + \frac{\partial u_2}{\partial x}\right)\right) + F_1 \qquad (2)$$

$$\rho\left(\frac{\partial u_2}{\partial t}+u\frac{\partial u_2}{\partial x}+v\frac{\partial u_2}{\partial y}\right)$$
$$=-\frac{\partial p}{\partial y}+2\mu\frac{\partial^2 u_2}{\partial y^2}+\frac{\partial}{\partial x}\left(\mu\left(\frac{\partial u_1}{\partial y}+\frac{\partial u_2}{\partial x}\right)\right)-\rho g+F_2 \quad (3)$$

where t is time, x is the horizontal distance from the wavemaker, y is the vertical height from the SWL and increases with depth, u_1 is the horizontal flow velocity, u_2 is the vertical flow velocity, F_1 is the horizontal force on the fluid, F_2 is the vertical force on the fluid, p is pressure and μ is viscosity.

In order to determine the position of the free surface, or air-water boundary, the volume of fluid method is applied. This technique was also employed by Liang et al (2010). This method adds another governing equation, given by:

$$\frac{\partial q_i}{\partial t}+u_1\frac{\partial q_i}{\partial x}+u_2\frac{\partial q_i}{\partial y}=0, i=1,2 \quad (4)$$

where q_i is the volume fraction of the fluid i with $\sum_{i=1}^{2} q_i = 1$. The free surface is then approximated as at the position of the minimum of value $|q_1 - q_2|$ along the model.

2.2. Optimisation of the length/height of the model

The height of the model is dictated by a number of factors; the still water level, the maximum height of the waves and the response amplitude and height of the device. Therefore, since the tank is being designed for deep water wave theory, the height of the tank is estimated to be 4/3 times the still water level, as this will leave sufficient room at the top (Opening boundary) of the tank for the device to oscillate as a result of the incoming wave.

As it is a numerical model, the geometry of the wave tank can be easily changed. As a result of this, the geometry can be optimised depending on the period of the incoming wave. As the incoming waves

will be almost linear, Linear (Airy) wave theory can be used to predict the minimum depth of the water, as follows (Coastal Engineering Research, 1977):

$$\frac{d}{L_0} > \frac{1}{2} \tag{5}$$

where $L_0 = \frac{gT^2}{2\pi}$, g is gravity and T is the wave period. Thus, Eq. (5) can be written as:

$$d > \frac{gT^2}{4\pi} \tag{6}$$

This relationship between the minimum still water level, d, and the wave period, T, is shown graphically in **Fig. 2**.

The length of the model is dictated by the SWL, the beach slope and the size of the WEC device being investigated. Dean and Dalrymple (1984) show that the velocity potential for a 2-D wavemaker is divided into two parts; the first is that of the progressive wave and the second of the standing wave, which decay away from the wavemaker. It is also shown that the standing wave part is negligible after a distance of three times the SWL, or *3d*, away from the wavemaker. Therefore, from this distance onwards the progressive wave is only present and, as a result, the optimum placing of a device in a wavetank is at this distance. An illustrated summary of these dimensioning techniques is shown in **Fig. 1**.

2.3. Optimisation of the model mesh

It is essential to optimise the mesh size as this will reduce computational effort. This is particularly important for 3-D modelling of wave tanks. A significant observation that must be noted is the sensitivity of the wave elevation to the mesh refinement. Therefore, it is essential to optimise the method of meshing employed, which should be dependent on the height and period of the wave being created.

In **Table 1** and **Fig. 3**, a number of meshing techniques are compared in order to determine which method would provide the most optimum mesh. The generated wave used in the comparison has a period of *1.35s*, and it adheres to finite depth theory, as *d = 1.5m*. A beach slope of 1:5 is employed. The variables used in the comparison in the comparison are: (1) the mesh relevance, which defines the fineness of the overall mesh, (2) the maximum mesh element size and (3) the radius of the *'Sphere of Influence'* being used and its element size. The *'Sphere of Influence'* technique is employed in order to perform mesh refinement along the SWL, between the wavemaker and the beginning of the beach.

From **Fig. 3**, it is clear that the most efficient mesh is that in model WT2, which contained 4830 elements, as it provides a wave that is insignificantly different to that obtained from model WT4, which contained 6440 element mesh. Therefore, the optimum mesh for the model utilises both a maximum element size and the *'Sphere of Influence'* technique.

During the study, it was found that the radius of the sphere is dependent on the height of the wave and, as a result, the radius is estimated as the expected height of the wave and an element size of one tenth the radius is sufficient. The optimum minimum element size was established in this study, i.e. for *T = 1.35s*, and is affected by the wavelength, L_0. Therefore, a simple linear relationship was established to estimate the minimum element size when *T = n sec* and is given as:

$$Min.\,Element\ Size = \frac{L_0[T = n\ sec]}{L_0[T = 1.35\ sec]} x0.15m \qquad (7)$$

This relationship holds true when the beach slope is at 1:5 and the meshing method above is adhered to. A typical mesh for the model is shown in **Fig. 4**.

2.4. Time-step interval and total time

The time-step interval and total time are both dependent on the wave period. As the device is being placed at three times the still water level, *3d*, the waves of interest are those at this location. From **Fig. 5**, it is clear that waves of various periods are fully developed at this location after six cycles.

Therefore, a total time equal to ten times the wave period is sufficient to allow comparison between the waves generated by the numerical model and their predicted by LWT and WMT, with the waves created during the last four cycles being those of interest, i.e. fully developed waves.

Furthermore, a parametric study was carried out in order to determine the optimum integration time-step interval. As accurate velocity results are one of the main requirements from the simulation, it is necessary to use a relatively small integration time-step interval. The results of this parametric study are shown in **Fig. 6** and it is clear that the optimum time-step is found by dividing the wave period into 50 intervals (T/50). This agrees closely with the findings of Ning and Teng (2007), which stated the maximum time-step interval is the wave period divided by 40 (T/40).

3. Results

3.1. Beach Slope Study

A variety of techniques have been employed by a number of researches to dissipate, or damp out, the waves at the end of the model. Ning and Teng (2007) and Ning et al (2008) used an artificial beach employed along the free surface boundary of the model. Liang et al (2010) introduced a dissipation zone by adding terms to the momentum equations in order to eliminate wave reflection. In this study, a sloped beach is used to damp out the waves, a technique which is also used by Lal and Elangovan (2008).

The optimum beach slope to provide damping of the wave at the end of the model is explored over a variety of slopes. The mesh sensitivity, discussed in Section 2.2, is used as an advantage near the beach, as a coarse mesh will produce a damping effect on the wave. This technique is also employed by Park et al (1999) and Park et al (2004) in the dissipation zone as the mesh becomes coarser horizontally along the zone.

Models with beach slopes ranging from 1:3 to 1:6 were investigated. The measured transient wave elevations for various beach slopes at 1.5m from the end of the beach are plotted in **Fig. 7**. A distance of 1.5m from the end of the beach was chosen as it was a monitoring point near the end of the beach, which was without the presence of nonlinearities as a result of the wave breaking. It was found that the optimum beach slope is 1:5, as the difference in the degree of damping provided compared to a slope of 1:6 is negligible. This result contradicts the findings of Lal and Elangovan (2008), where an optimum beach slope of 1:3 was determined. As can be seen in **Fig. 7**, a model containing a beach slope of 1:3 would induce the least damping of the slopes investigated. A comparison between the wave elevation of the fully formed progressive wave and the dissipated wave, near the end of the beach, is shown in **Fig. 8**. It is clear to see that damping of the wave has occurred as a result of the sloped beach. The generated wave used in this study is the same as the one used in Section 2.2 and employs the optimum mesh method.

3.2. Validation of CFD wave with LWT

The validation of the method required is a vital step in this analysis. The first validation is a comparison of the generated wave in terms of the water particle velocity, v, between the SWL and model base, to linear wave theory (LWT), which uses the following set of equations (Coastal Engineering Research, 1977):

$$v = A\omega e^{k_0 y} \tag{8}$$

$$\eta_{LWT} = A\cos(\varepsilon_0 + \omega t) \tag{9}$$

where v is the water particle velocity, A is the wave amplitude, ω is the angular frequency of the wave, $k_0 = \omega^2/g$ is the wavenumber for the deep water case, y increases from the SWL with depth, η_{LWT} is the wave elevation of the LWT wave, and ε_o is the initial phase angle dependant on the initial stroke of the wavemaker and the distance from the wave maker of the profile.

Fig. 9 (a) shows that the wave elevation of the CFD generated deep water wave is identical to that for the LWT wave once the CFD wave has fully developed. **Fig. 9** (b) compares the scalar water particle velocity of the CFD wave, which is labelled *'Velocity'*, and scalar water particle velocity according to LWT, which is labelled *'LWT Velocity (v)'*, which are, also, in very good agreement. Furthermore, the horizontal component of the water particle velocity, which is labelled *'Hor. Velocity'*, and the vertical component of the water particle velocity, which is labelled *'Vert. Velocity'*, of the CFD wave are displayed in **Fig. 9** (b). These are the vectors that combine to create the scalar wave particle velocity. Similarly, these comparisons and conclusions are true for the generated deep water wave in **Fig. 10**.

3.3. Validation of CFD wave with WMT

In **Fig. 11**, results from CFD analysis and WMT are plotted in terms of the wave height to stroke length ratio (H/S) against the wavenumber, k_0, times the height of the wavemaker flap hinge to SWL, where the hinge of the wavemaker flap is at the base of the tank. It was found that for the deep water case, a flap type wavemaker hinged at the bottom of the model does not satisfy wavemaker theory for deep water waves, which is valid for $k_0h \geq 3.13$ according to LWT. On the other hand, it is satisfied when $k_0h \leq 2$, where h is the height of the wavemaker hinge to the SWL. Hence, this only holds true for the finite/shallow depth case according to LWT and this can clearly be seen in **Fig. 11**. Therefore, it is necessary to adapt the model to satisfy both linear theory and wavemaker theory. This is achieved by moving the hinge of the wavemaker to a distance of half the still water level, $h/2$, above the base of the model. However, from **Fig. 12**, it can be seen that this adaption is only valid for a $k_0h \leq 1.7$. Consequently, as $2h = d$, the theory is valid for the deep water case provided the relation k_0h does not exceed 1.7.

As the hinge of the wavemaker flap is located at a distance of half the SWL above the base of the model, it is necessary to adapt the theory in order to allow for the section of the wavemaker wall that is now stationary. Wavemaker theory, when generating two-dimensional small amplitude waves, is derived from the velocity potential of a simple boundary value problem. This velocity potential, ϕ,

describes the simple harmonic wave motion. The boundary conditions which need to be satisfied are: the Laplace's equation, the free surface condition, the structural boundary condition, the base condition and the radiation condition, respectively (Linton and McIver, 2001):

$$\nabla^2\varphi = \frac{\partial^2\varphi}{\partial x^2} + \frac{\partial^2\varphi}{\partial y^2} = 0 \tag{10}$$

$$\omega^2\varphi - \mathrm{g}\frac{\partial\varphi}{\partial \mathrm{y}} = 0 \; on \; y = 0 \tag{11}$$

$$\frac{\partial\varphi}{\partial \mathrm{x}} = U(y)\sin\omega t \;\; on \; x = 0 \tag{12}$$

$$\frac{\partial\varphi}{\partial \mathrm{y}} = 0 \; on \; y = d \tag{13}$$

$$\lim_{x\to\infty}\left(\frac{\partial\varphi}{\partial \mathrm{x}} \mp \mathrm{i}k_0\varphi\right) = 0 \tag{14}$$

where *U(y)* is the prescribed horizontal velocity of the wavemaker. This problem is solved by Ursell et al (1960), where the wave height to wavemaker stroke ratio (H/S) is given for a paddle wavemaker hinged at the base as:

$$\begin{aligned}\frac{H}{S} &= \frac{\omega^2\cosh k_0 h}{g k_0}\frac{\int_0^h\{1-y/h\}\cosh k_0(h-y)\,dy}{\int_0^h \cosh^2 k_0(h-y)\,dy} \\ &= \frac{4\sinh k_0 h}{k_0 h}\frac{k_0 h\sinh k_0 h - \cosh k_0 h + 1}{\sinh k_0 h + 2k_0 h}\end{aligned} \tag{15}$$

However, this takes the prescribed horizontal velocity of the wavemaker as:

$$U(y) = \frac{1}{2}S\omega\{1-y/h\} \tag{16}$$

Since, there is fluid now below the height of the hinge of the wavemaker, the wavemaker exerts a force on this fluid and, in turn, Eq. (15) needs to be adapted to show this loss of energy. Furthermore,

when the hinge of the wavemaker is taken at a height, *l*, from the base of model, the prescribed horizontal velocity of the wavemaker is given as:

$$U(y) = \frac{1}{2} S\omega\{1 - y/h\} \; at \; 0 \le y \le h - l \\ 0 \; at \; h - l \le y \le h \tag{17}$$

Therefore Eq. (15) is adapted to allow for this change in the height of the hinge to give:

$$\frac{H}{S} = \frac{\omega^2 \cosh k_0 h}{g k_0} \frac{\int_0^{h-l} \{1 - y/h\} \cosh k_0 (h - y) \, dy}{\int_0^h \cosh^2 k_0 (h - y) \, dy} \\ = \frac{4 \sinh k_0 h}{k_0 h} \frac{k_0 h \sinh k_0 h - \cosh k_0 h - k_0 l \sinh k_0 l + \cosh k_0 l}{\sinh k_0 h + 2 k_0 h} \tag{18}$$

where, *h* is the height of the wavemaker from the hinge to the still water level, k_0 is obtained from the relation $\omega^2 = g k_0 \tanh k_0 h$, and *l* is the height of the hinge of the wavemaker from the base of the model. The above equation is represented by the *'WMT Curve'* in **Fig. 12**. It is evident from **Fig. 12** that the theory is valid for the deep water case with the wavemaker hinged at a height of half the still water level, h, provided the relation $k_0 h$ does not exceed 1.7.

3.4. Comparison of turbulence models

A comparison was carried out between a laminar and a k-ε turbulence model in order to investigate the effects of viscosity. The k-ε turbulence model includes the history effects such as the turbulent kinetic energy and turbulent dissipation. However, it was found that there was no difference in the generated wave elevation between the two models and, therefore, is not a factor in the generation of water waves using a wavemaker. Similar observations are noted by Lal and Elangovan (2008).

3.5. Scaling laws in deep water wave modelling

There is a dimension restriction in ANSYS CFX (Version 12.1) of 500 m (ANSYS, 2009). Therefore, as a result of the model dimensions derived in this paper, it is necessary to scale the model when dealing with low frequencies (i.e. $f \leq 0.125$). Furthermore, when dealing with real-world models it is necessary to use the scaling factors derived in this section. These scaling factors are derived from the equations used in linear (Airy) wave theory for deep water waves (Coastal Engineering Research, 1977). A summary of the scaling factors is given in **Table 2**. Please note that these are not all of the scaling factors, but a summary of those applicable to deep water wave modelling.

The scaling that is referred to in this paper is a function of the wave period, T, and the scaling coefficient is s, where $T_{new} = s\,T_{in}$. As force is directly proportional to acceleration and acceleration is given as $A\omega^2 e^{ky}$ (Coastal Engineering Research, 1977), it is deduced that the wave force on a body/structure is given by the relation:

$$F_{new} = \frac{F_{in}}{s^2} \tag{19}$$

where, F_{new} is the wave force on the body or structure in the scaled model, F_{in} is the wave force on the full scale body or structure and s is the scaling coefficient.

4. Wave-Structure Interaction

In this section, the methodology described in Sections 2 and 3 is used to analyse the interaction between a linear wave and a floating truncated vertical cylinder. For this analysis, two simulations are required. The first is when the structure is held in a fixed position in order to obtain the excitation force. The second is when the structure is free to oscillate in the vertical, or heave, motion.

Since the model is to represent deep water conditions, i.e. infinite depth, it is necessary to increase the depth of the water. This change to the methodology is required as the oscillating body generates fluid velocities beneath it and these velocities are affected by the base of the model if the depth isn't sufficient. When specifying the boundary conditions on the longitudinal walls of the model, a

symmetry boundary is specified on one wall in order to only model half of the problem and reduce the calculation required. On the other longitudinal wall, a wall with an unspecified mesh motion and no symmetry is specified. The free surface and a fixed floating cylinder of the model are shown, for example, in **Fig. 13** for a specific moment in time.

In the initial analysis, the cylinder is held in a fixed position and the excitation forces are calculated. The CFD solution will be compared to an analytical solution derived by Finnegan et al (2011) in order to ensure the CFD analysis is setup and performing accurately. Finnegan et al (2011) employs the method of separation of variables in order to derive the velocity potential in the fluid domain for calculating the wave excitation forces on a floating truncated vertical cylinder in water of infinite depth. The vertical, or heave, excitation force, in the frequency domain, $\hat{F}_{3,ext}$, is given as (Finnegan et al, 2011):

$$\hat{\mathrm{F}}_{3,\mathrm{ext}} = -2\pi i\rho\omega a\sqrt{\frac{2}{\pi}}\int_0^\infty p_0(\xi)\frac{I_1(\xi a)}{\xi I_0(\xi a)}\,d\xi \tag{20}$$

and

$$p_0(\xi) = -\frac{gA}{\omega}i\sqrt{\frac{2}{\pi}}\left(J_0(k_0a) + J_0{}'(k_0a)\frac{H_0^{(1)}(k_0a)}{H_0^{(1)\prime}(k_0a)}\right)\frac{e^{-k_0b}k_0}{\xi^2 + {k_0}^2} \tag{21}$$

where p_0 is a coefficient, a is the radius of the cylinder, b is the draft of the cylinder, I_m is the modified Bessel function of the first kind of order m, J_m is the Bessel function of the first kind of order m, $H_m^{(1)}$ is the Hankel function of the first kind of order m, and ξ is the separation constant.

A time-domain comparison between the analytical and CFD results is shown for a dimensionless wavenumber, k_0a, of 0.6 with a draft to radius ratio of $a = b$ and $a = 2b$, in **Fig. 14** and **Fig. 15**, respectively. The maximum heave excitation forces in both are slightly overestimated in the analytical approximation and there is a slight phase difference between the two approaches. In addition, a parametric study for different dimensionless wavenumbers, k_0a, is performed for a draft to radius ratio

of $a = b$ and $a = 2b$. In this study, the analytical and the CFD results match up closely, as shown in **Fig. 16**.

From the second simulation, where the cylinder is free to move in the vertical direction, the dynamic response and the hydrodynamic force, or total wave force, on the structure is obtained. From this information, the total force on the structure can be decomposed into the various forces. Since the model deals with an unrestrained system, i.e. there are no external mechanical forces applied to the structure, the total wave force is the hydrodynamic force, which can be summarised as follows:

$$F_H = F_{ext} + F_R + F_{hs} = -M\frac{d^2y}{dt^2} \tag{22}$$

Where F_H is the hydrodynamic force, F_{ext} is the excitation force, F_R is the radiation force, F_{hs} is the hydrostatic force, M is mass of the body, and y is the dynamic displacement response of the structure, which increases from the SWL with depth. For preliminary models of WEC's, it is reasonable to assume the excitation force is a combination of the Froude-Krilloff force and the diffraction force. This assumption is only valid when the overall dimensions are large compared to the wave length and Keulegan-Carpenter parameter (Dean and Dalrymple, 1984) is less than one. Furthermore, by using **Eqn. (22)**, the total hydrodynamic force may be separated into the various forces which comprised it. An example of a summary of these forces is shown graphically, in the time-domain, for a case study in **Fig. 17**.

The case study, which is detailed in this section, is a floating truncated vertical cylinder, with $a = b = 0.6m$, and an incident wave of period $2s$ and an amplitude of $0.08m$. A time domain representation of the incident wave and the dynamic response of the body is shown in **Fig. 18**. The excitation force on the body is shown in **Fig. 14** and the summary of the forces which make up the hydrodynamic force is shown in **Fig. 17**. Furthermore, the added mass and the wave damping may be calculated from the radiation force which is given, in the frequency domain, as:

$$\hat{F_R} = -\ddot{y}a_m - \dot{y}v = \omega^2 y a_m + i\omega y v \tag{23}$$

Where a_m is the added mass and ν is the wave damping. For the given case study the added mass is calculated as $196\ kg$ and the wave damping is calculated as $185\ kg/s$.

5. Discussions and Conclusions

A guide to designing a CFD model that can accurately produce both linear deep water waves and linear waves for the finite depth case was presented in this paper. Furthermore, steps required to be taken to design an optimum CFD model were outlined. In particular, the effects of the meshing method, beach slope angle and the total time and time-step interval for the transient analysis set-up were explored, while minimising the overall dimensions of the model to generate a deep water wave.

The optimum mesh for the model utilises both a maximum element size and the *'Sphere of Influence'* technique. A total time equal to ten times the wave period was found to be sufficient and the optimum time-step interval is to divide the wave period into 50 intervals (T/50), which can be seen in **Fig. 6**. It is recommended to use a beach slope of 1:5 to dissipate, or damp out, the waves at the end of the wave tank.

Furthermore, it is evident from **Fig. 11** and **Fig. 12** that a limitation of ANSYS CFX is it can only conform to WMT when dealing with relatively low k_0h values, i.e. $k_0h \leq 2$ for $h = d$ and $k_0h \leq 1.7$ for $2h = d$. It can also be concluded from **Fig. 12** that, only when the hinge of the wavemaker is raised, can deep water waves be generated and conform to both WMT, using the adapted version of the equation described in Ursell (1960), and LWT. **Fig. 9** and **Fig. 10** show two sets of comparisons and from these it is apparent that the CFD generated deep water wave is in very good agreement to LWT. Therefore, the aim of generated linear regular waves in a wavetank model using a commercial CFD software package, ANSYS CFX, has been achieved.

Finally, a case study of the interaction of a linear deep water wave and a floating truncated vertical cylinder, which employs the methodology to create a NWT described in this paper, is undertaken. A comparison between the CFD analysis and an analytical solution was undertaken to ensure the accuracy of the model set-up. It was found that the response predictions from the analytical and CFD model match up closely. Furthermore, a floating truncated vertical cylinder that oscillates in the

vertical, or heave, motion was analysed to give the dynamic response and hydrodynamic forces on the structure. The added mass and wave damping were calculated from the radiation force.

Acknowledgements

The first author would like to acknowledge the financial support from the National University of Ireland under the College of Engineering & Informatics Postgraduate Fellowship. The authors would also like to express their gratitude to the anonymous reviewers of this paper for their constructive comments.

References:

Agamloh E.B., Wallace A.K., von Jouanne A., 2008. Application of fluid-structure interaction simulation of an ocean wave energy extraction device. Renewable Energy. 33(4): p. 748-757.

ANSYS-Inc., 2009. ANSYS CFX, Release 12.1. 2009.

Coastal Engineering Research Center, 1977. Shore protection manual / U.S. Army Coastal Engineering Research Center. Fort Belvoir, Va. Washington: Supt. of Docs., U.S. Govt. Print. Off.

Contento G., 2000. Numerical wave tank computations of nonlinear motions of two-dimensional arbitrarily shaped free floating bodies. Ocean Engineering. 27(5): p. 531-556.

Dean R.G., Dalrymple R.A., 1984. Water wave mechanics for engineers and scientists Englewood Cliffs, N.J.: Prentice-Hall.

Finnegan W., Meere M., Goggins J., The Wave Excitation Forces on a Floating Vertical Cylinder in Water of Infinite Depth, in World Renewable Energy Congress 2011. 2011: Linkoping Sweden.

Hadzic I., Hennig J., Peric M., Xing-Kaeding Y., 2005. Computation of flow-induced motion of floating bodies. Applied Mathematical Modelling. 29(12): p. 1196-1210.

Kim M.H., Niedzwecki J.M., Roesset J.M., Park J.C., Hong S.Y., Tavassoli A., 2001. Fully Nonlinear Multidirectional Waves by a 3-D Viscous Numerical Wave Tank. Journal of Offshore Mechanics and Arctic Engineering. 123(3): p. 124-133.

Koo W., Kim M.H., 2004. Freely floating-body simulation by a 2D fully nonlinear numerical wave tank. Ocean Engineering. 31: p. 2011-2046.

Lal A., Elangovan M., 2008. CFD Simulation and Validation of Flap Type Wave-Maker. World Academy of Science, Engineering and Technology. 46: p. 7.

Liang X.-f., Yang J.-m., Li J., Xiao L.-f., Li X., 2010. Numerical Simulation of Irregular Wave-Simulating Irregular Wave Train. Journal of Hydrodynamics, Ser. B. 22(4): p. 537-545.

Linton C.M., McIver P., 2001. Handbook of Mathematical Techniques for Wave/Structure Interactions. Boca Raton, FL: Chapman & Hall/CRC.

Mousaviraad S.M., Carrica P.M., Stern F., 2010. Development and validation of harmonic wave group single-run procedure for RAO with comparison to regular wave and transient wave group procedures using URANS. Ocean Engineering. 37(8-9): p. 653-666.

Ning D.Z., Teng B., 2007. Numerical simulation of fully nonlinear irregular wave tank in three dimension. International Journal for Numerical Methods in Fluids. 53: p. 1847-1862.

Ning D.Z., Teng B., Eatock Taylor R., Zang J., 2008. Numerical simulation of non-linear regular and focused waves in an infinite water-depth. Ocean Engineering. 35(8-9): p. 887-899.

Park J.-C., Kim M.-H., Miyata H., 1999. Fully non-linear free-surface simulations by a 3D viscous numerical wave tank. International Journal of Numerical Methods in Fluids. 29: p. 685-703.

Park J.C., Uno Y., Sato T., Miyata H., Chun H.H., 2004. Numerical reproduction of fully nonlinear multi-directional waves by a viscous 3D numerical wave tank. Ocean Engineering. 31(11-12): p. 1549-1565.

Sriram V., Sannasiraj S.A., Sundar V., 2006. Simulation of 2-D nonlinear waves using finite element method with cubic spline approximation. Journal of Fluids and Structures. 22(5): p. 663-681.

Sun H., Faltinsen O.M., 2006. Water impact of horizontal circular cylinders and cylindrical shells. Applied Ocean Research. 28(5): p. 299-311.

Turnbull M.S., Borthwick A.G.L., Eatock Taylor R. 2003. Wave-structure interaction using coupled structured-unstructured finite element meshes. Applied Ocean Research. 25(2): p. 63-77.

Ursell F., Dean R.G., Yu Y.S., 1960. Forced small-amplitude water waves: a comparison of theory and experiment. Journal of Fluid Mechanics. 7(01): p. 33-52.

Versteeg H.K., Malalasekera W., 1995. An Introduction to Computational Fluid Dynamics. The Finite Volume Method: Longman Group Ltd.

Wu G.X., Hu Z.Z., 2004. Simulation of nonlinear interactions between waves and floating bodies through a finite-element-based numerical tank. Proceedings of the Royal Society of London. Series A: Mathematical, Physical and Engineering Sciences. 460(2050): p. 2797-2817.

Yan H., Liu Y., 2011. An efficient high-order boundary element method for nonlinear wave-wave and wave-body interactions. Journal of Computational Physics. 230(2): p. 402-424.

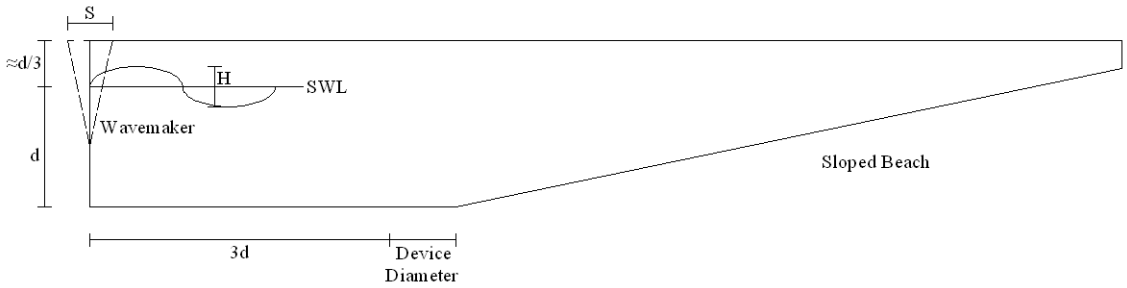

Fig. 1 Overall dimensions of model

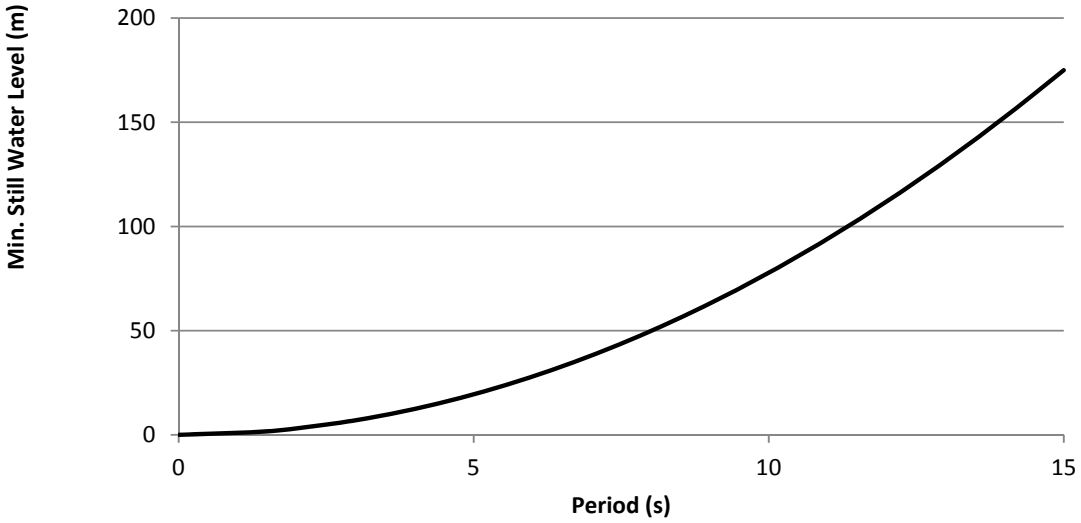

Fig. 2 Minimum still water level as the wave period varies

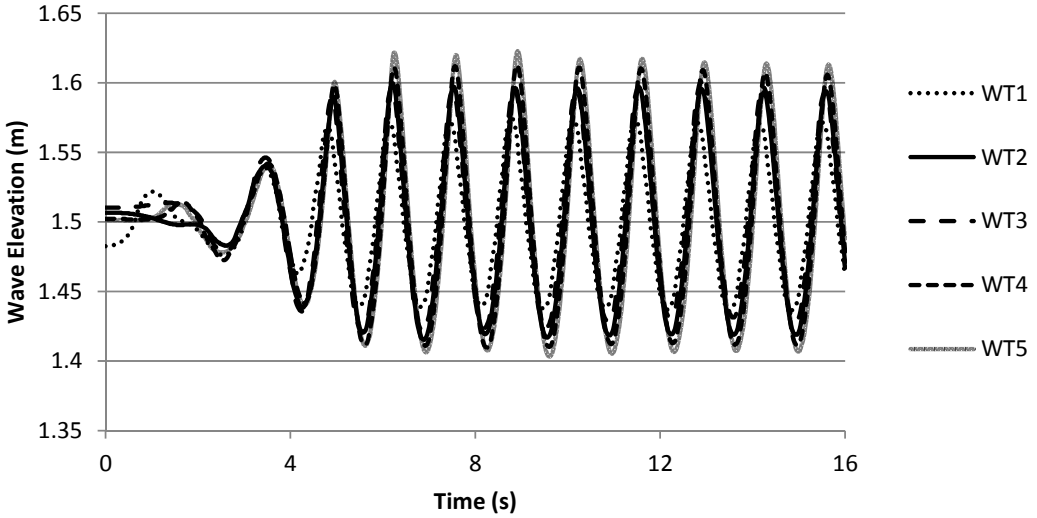

Fig. 3 Comparison of wave elevation at 5m, or 3d, from the wavemaker for various mesh set-ups given in Table 1

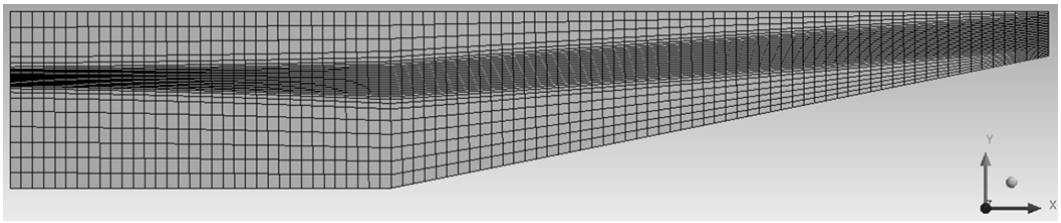

Fig. 4 Typical mesh for a wave tank model

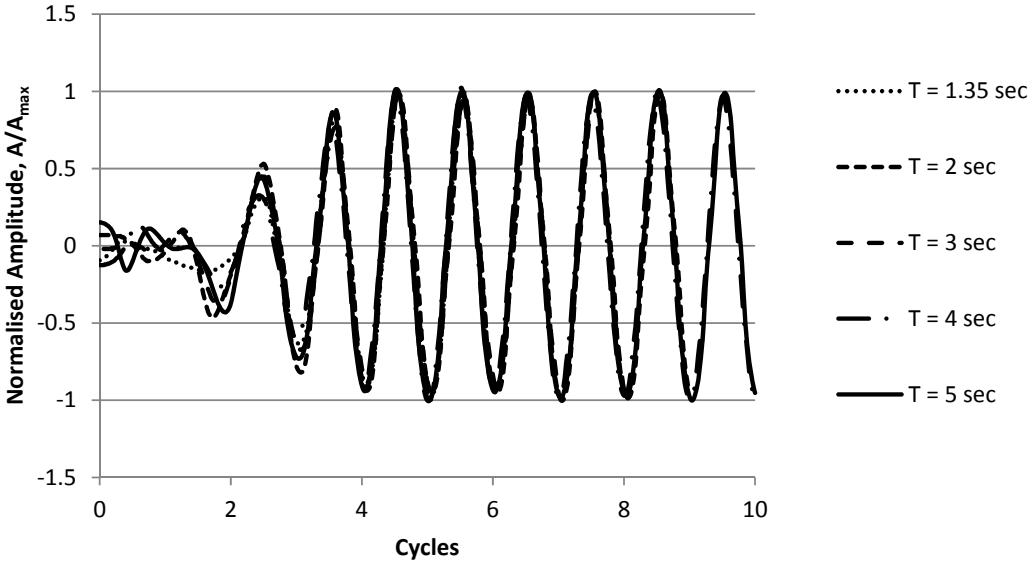

Fig. 5 The normalised amplitude wave profile for various wave periods at a distance 3d from the wavemaker for the first ten cycles

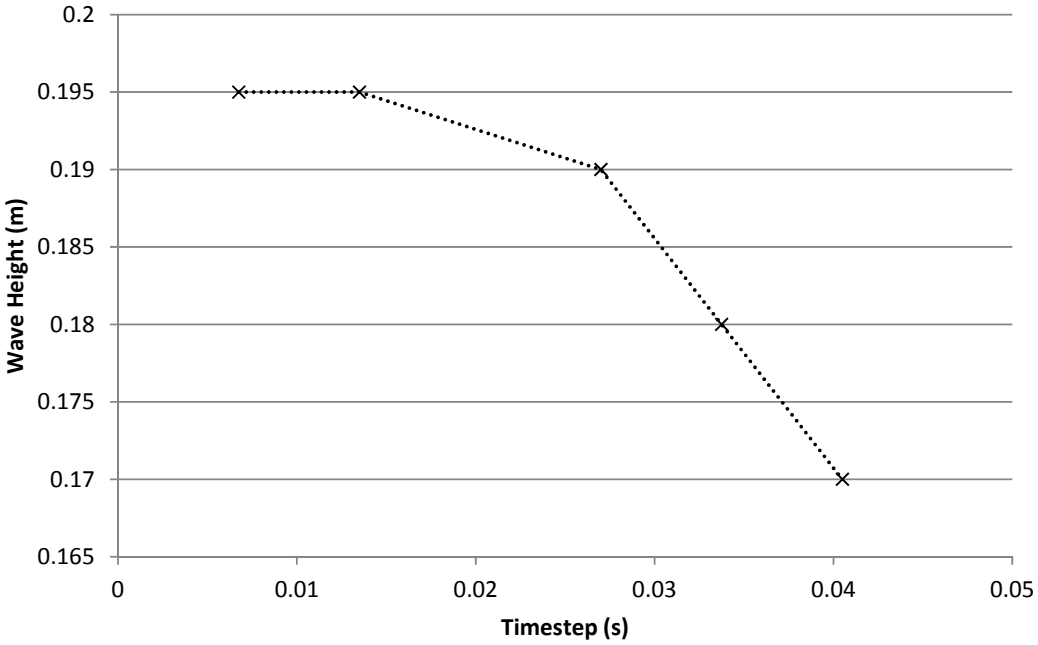

Fig. 6 Results from a parametric study comparing the effect of the time-step on the wave height for a wave period of 1.35s

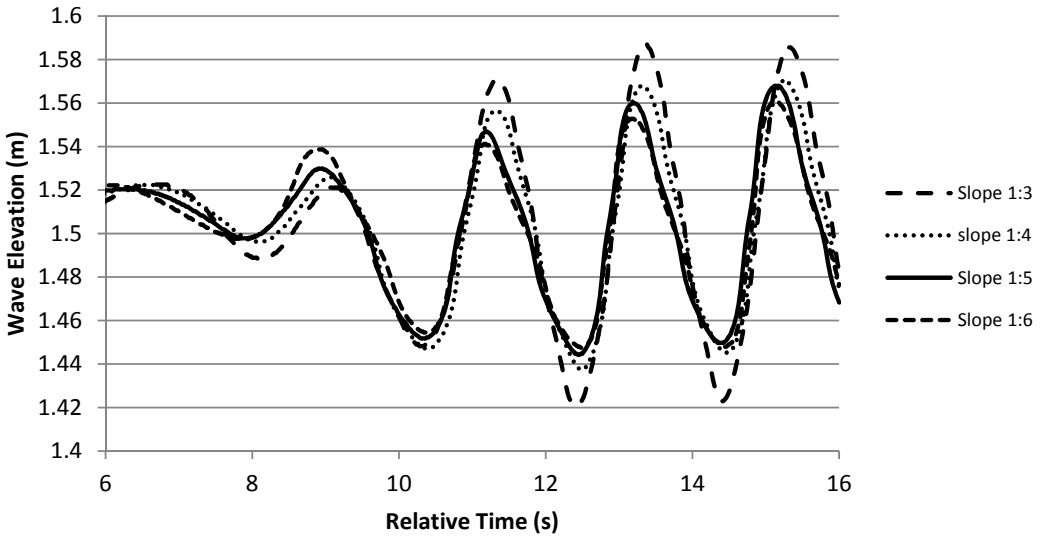

Fig. 7 A comparisons of the wave elevations for various beach slopes at 1.5m from the end of the beach

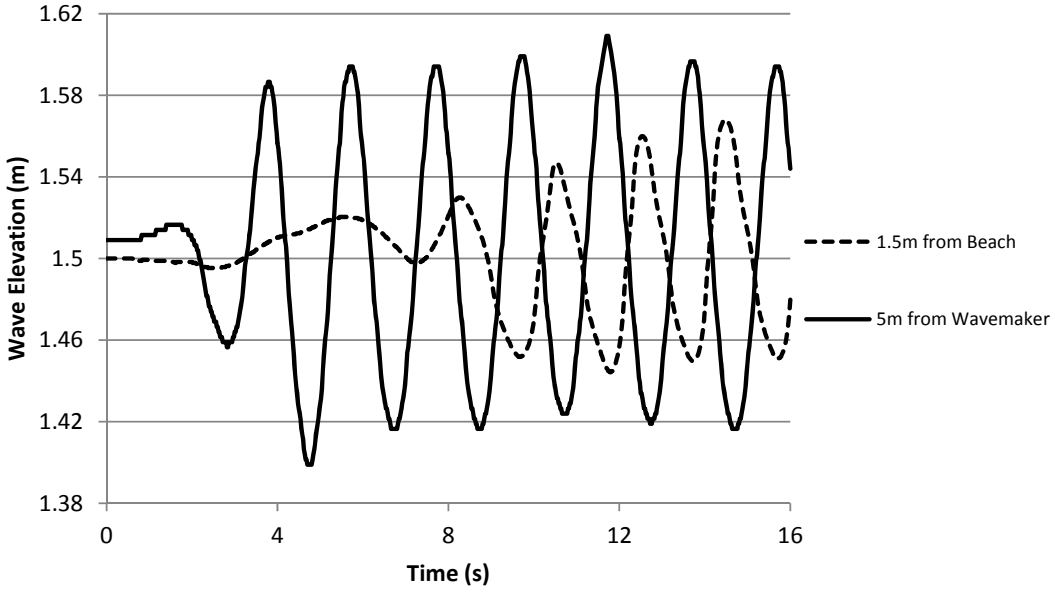

Fig. 8 A comparison of the wave elevation at 5m from the wavemaker and 1.5m from the end of the beach

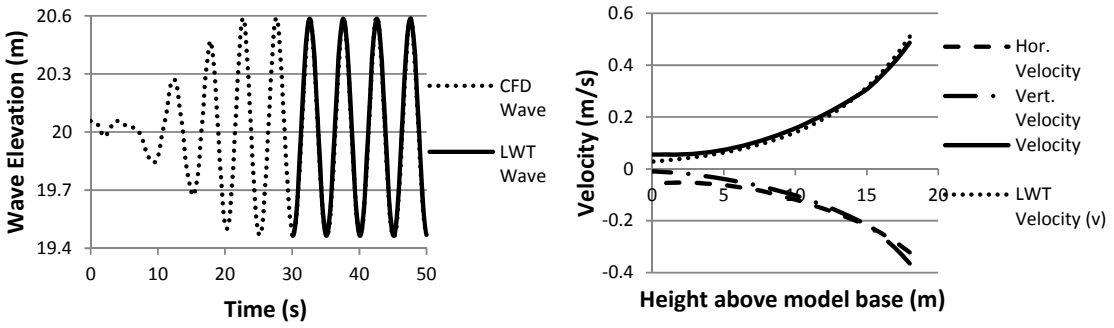

(a) *(b)*

Fig. 9 For a wave period of 5 s and a wave height of 1.12 m (i.e. 0.03L_0) and at a distance of 60m, or 3d from the wavemaker (a) Comparison of wave elevations of CFD generated wave to a linear wave (b) Comparison of CFD water velocity to LWT velocity for deep water

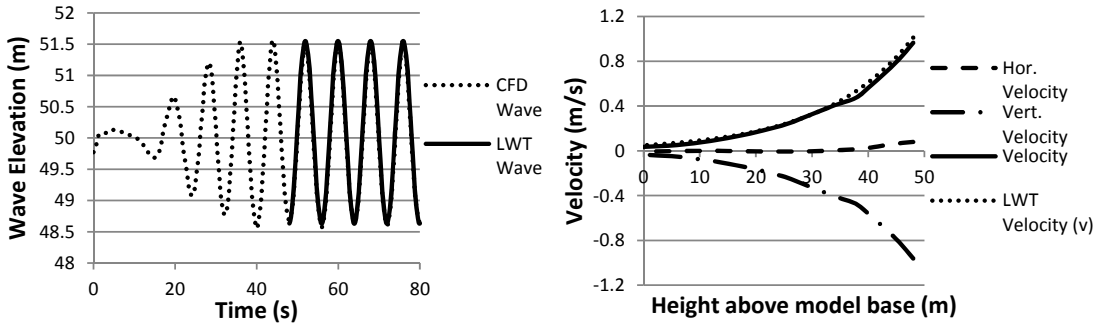

(a) *(b)*

Fig. 10 For a wave period of 8 s and a wave height of 2.92 m (i.e. 0.03L_0) and at a distance of 150m, or 3d from the wavemaker (a) Comparison of wave elevations of CFD generated wave to a linear wave (b) Comparison of CFD water velocity to LWT velocity for deep water

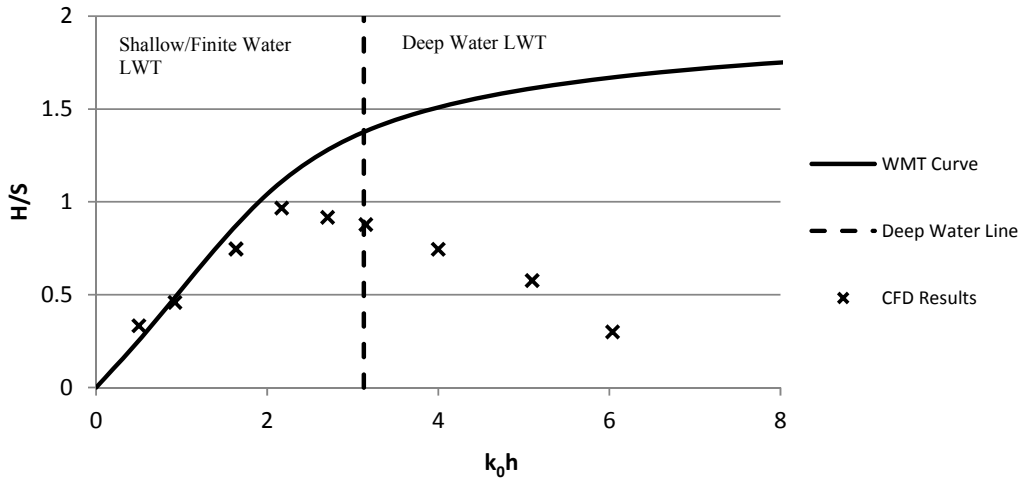

Fig. 11 Comparison of CFD results to wavemaker theory (WMT) for the wavemaker flap hinged at the base of the model

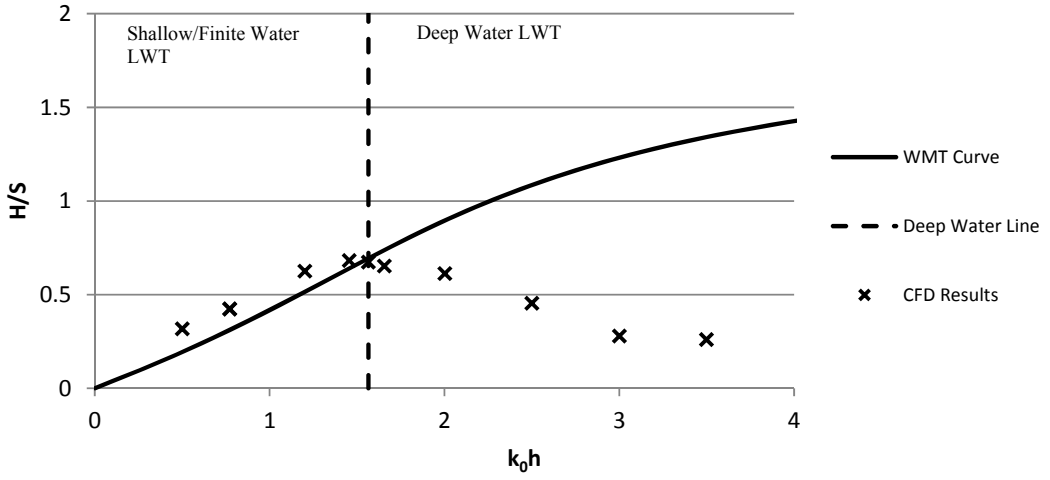

Fig. 12 Comparison of CFD results to wavemaker theory (WMT) with the wavemaker hinged at a height, l = 0.5d, from the base of the model

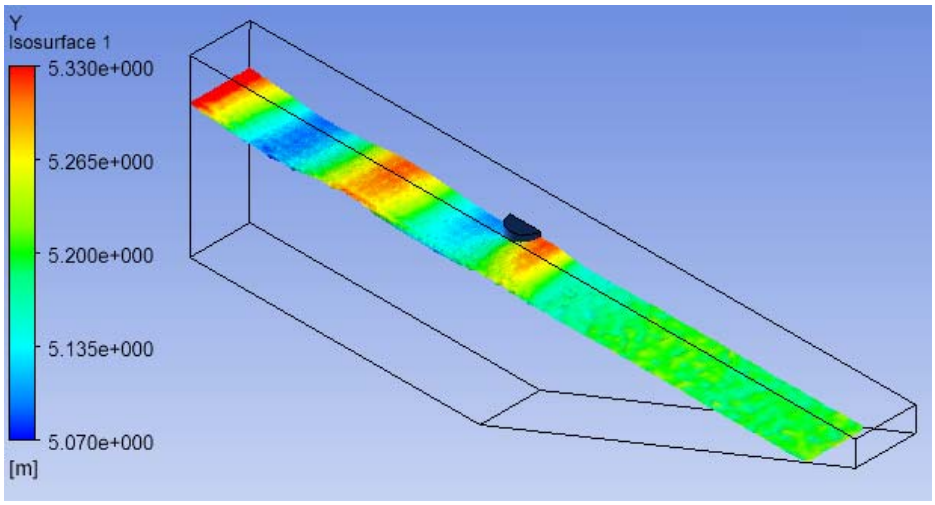

Fig. 13 The wave-structure interaction from CFD analysis (ANSYS CFX) after 24 seconds. The free surface and a fixed floating cylinder are shown.

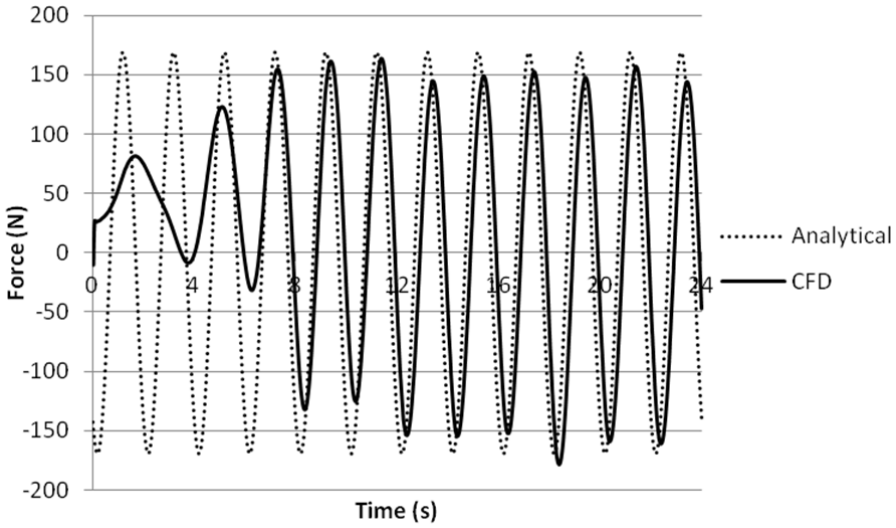

Fig 14 Time domain comparison between the heave excitation forces obtained from the analytical and CFD models with $k_0a = 0.6$ and $a = b$

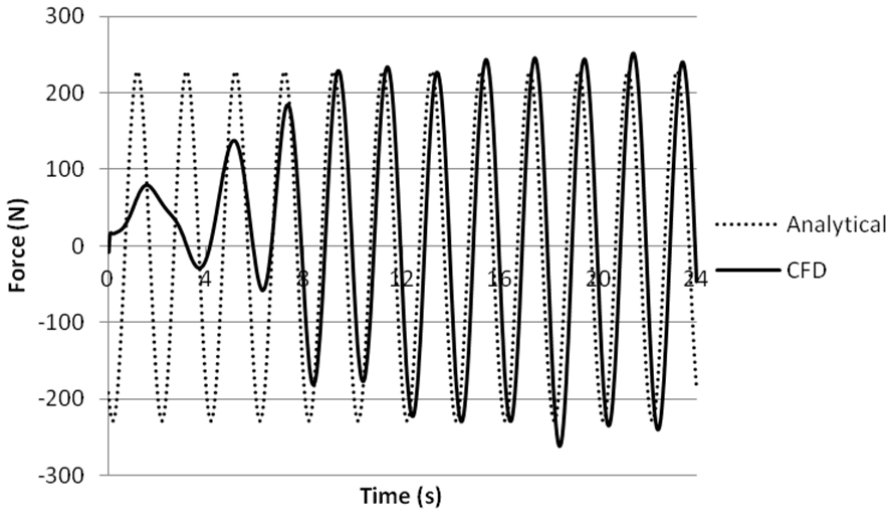

Fig 15 Time domain comparison between the heave excitation forces obtained from the analytical and CFD models with $k_0a = 0.6$ and $a = 2b$

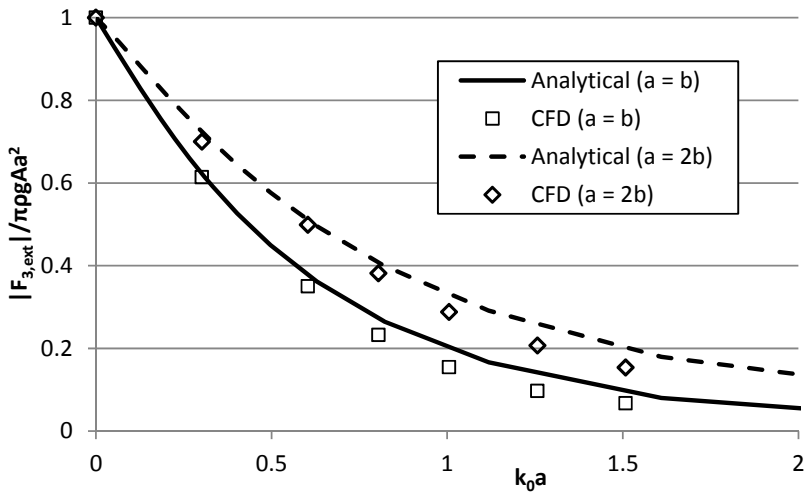

Fig. 16 Comparison of the normalised vertical, or heave, excitation force for the analytical and CFD models with ratios of $a = b$ and $a = 2b$

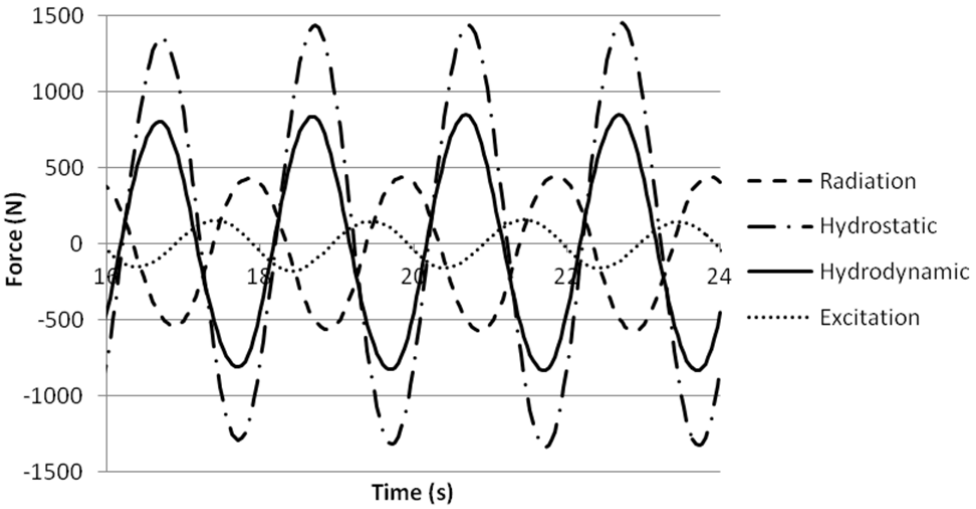

Fig. 17 Summary of the various forces on a floating truncated vertical cylinder with a=b, which is allowed to oscillate in a vertical, or heave, motion

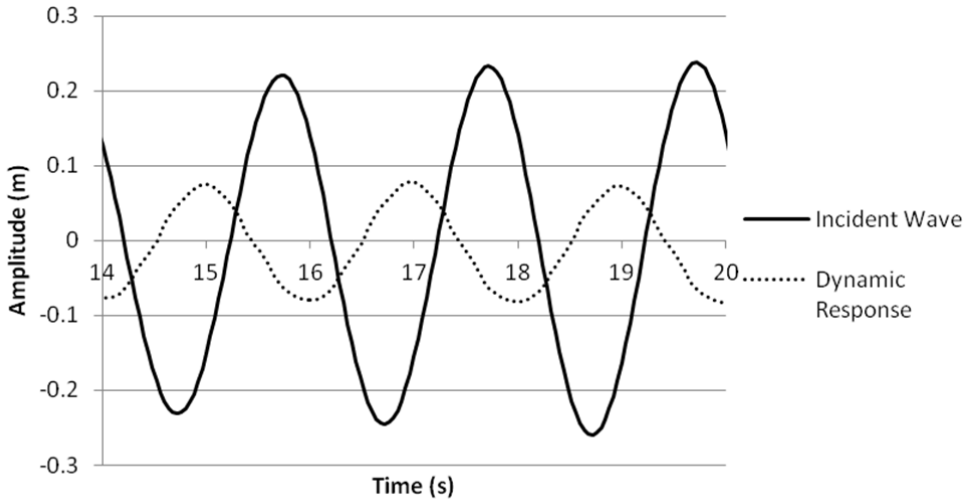

Fig. 18 The incident wave and the dynamic response of a floating truncated vertical cylinder with a=b, which is allowed to oscillate in a vertical, or heave, motion

Table 1. Summary of parametric study of mesh set-up

Model I.D.	No. of Elements	Relevance	Max. Element Size	Sphere of Influence		Wave Height
				Radius	Element Size	
WT1	2424	Fine 100	Undefined	0.3 m	0.02 m	0.125 m
WT2	4830	Fine 0	0.15 m	0.2 m	0.02 m	0.18 m
WT3	6231	Fine 100	0.12 m	0.3 m	0.02 m	0.17 m
WT4	6440	Fine 0	0.15 m	0.2 m	0.01 m	0.19 m
WT5	8900	Fine 0	0.15 m	0.2 m	0.005 m	0.2 m

Table 2 Summary of applicable scaling factors in deep water wave modelling. The subscript 'in' refers to the initial model and the subscript 'new' refers to the scaled model.

Quantity	**Symbol**	**Scaled Relation**
Wave Period	T_{new}	sT_{in}
Wave Angular Frequency	ω_{new}	ω_{in}/s
Wave Length	L_{new}	s^2L_{in}
Wave Amplitude	A_{new}	A_{in}
Water Mass	m_{new}	m_{in}
Water Density	ρ_{new}	ρ_{in}
Still Water Level	d_{new}	s^2d_{in}
Water Particle Velocity	v_{new}	v_{in}/s
Water Particle Acceleration	a_{new}	a_{in}/s^2
Wave Force on a Body/ Structure	F_{new}	F_{in}/s^2